J Appl Electrochem (2011) 41:257–270
DOI 10.1007/s10800-010-0234-3

REVIEW ARTICLE

Electrodeposition: a versatile and inexpensive tool for the synthesis of nanoparticles, nanorods, nanowires, and nanoclusters of metals

U. S. Mohanty

Received: 6 February 2010 / Accepted: 24 October 2010 / Published online: 4 November 2010

Abstract The synthesis of various nanoscale materials, such as nanoparticles, nanowires of Au, Pt, Ni Co, Fe, Ag etc., by electrodeposition techniques have been demonstrated in this article. Both potentiostatic and galvanostatic methods were employed to carry out the electrodeposition process under different potential ranges, time durations, and current densities. The electrochemical behavior of the deposited nanoparticles on various substrates was investigated by cyclic voltammetric and chronoamperometric techniques. The synthesis of mono-dispersed gold (Au) nanoparticles on indium tin oxide (ITO) coated glass, preparation of Au nanorods on nanoporous anodic alumina oxide (AAO), formation of Au nanoclusters on polypyrrole-modified glassy carbon electrode and one-step electrodeposition of nickel nanoparticle chains embedded in TiO_2 etc. have been highlighted in this article. The potential applications of synthesized nanoparticles such as the role of maghemite (Fe_2O_3) in arsenic remediation, higher electrocatalytic activity of Ag nanoclusters for the reduction of benzyl chloride, and the role of C_{60} nanoparticle-doped carbon film in fabrication processes are also presented in this article.

Keywords Electrodeposition · Gold · Nanoparticles · Nanoclusters · Nanowires · Nickel · Platinum · Silver · Synthesis

U. S. Mohanty (✉)
Department of Material Science and Engineering,
National Cheng Kung University, Tainan, Taiwan
e-mail: suryaudit@yahoo.com

1 Introduction

Nanomaterials have wide range of applications in the fields of energy, environmental, and medical technologies due to their unique properties determined primarily by its size, composition, and structure. These materials have been of considerable interest to the scientists because of their unusual and fascinating properties [1–5]. Several techniques have been used for the synthesis of nanoparticles. Some of the commonly used techniques are sol–gel process [6, 7], hydrothermal precipitation [8], homogenous precipitation [9], and reverse micelles method [10, 11]. Similarly, Esparza et al. [12] used chemical reduction technique for the synthesis of nanometric gold particles. Radio-frequency co-sputtering technique and subsequent annealing at different temperatures have been employed by Serano and Pal [13] for the synthesis of gold nanoparticles (GNPs) in Al_2O_3 matrix. Yang et al. [14] synthesized GNPs and nanoplates [14] with controlled size and morphology employing UV radiation in the presence of citric acid and poly(vinyl pyrrolidone) at room temperature. Apart from the above described methods, a unique process termed electrodeposition produces nanoparticles with controlled characteristics, namely, size, morphology, and the composition. It is simple, fast, inexpensive, and among the most familiar binder-free techniques employed for the preparation of nanoparticles. The advantage of this technique is that the nanoparticle gets directly attached to the substrate, and in comparison to other techniques, the particle size, crystallographic orientation, mass, thickness, and morphology of the nanostructured materials can be controlled by adjusting the operating conditions and bath chemistry [15–18]. Recently, a review on the synthesis and electrochemical applications of GNPs [19] has been reported by Guo and Wang. Riley [20] reported that

electrochemistry offered an excellent means of contacting nanoparticles; it allowed one to investigate the influence of charge and potential on the particle properties and also for the development of sensor and solar cell devices in which electrochemistry was used to address the nanoparticle arrays.

Rao and Trivedi [21] presented a review article on the recent developments on the deposition of all platinum group metals (PGMs) both by chemical and electrochemical methods. In this article, they have mentioned the various uses of the deposited coatings with special emphasis on the functional uses in electrochemical technology of fuel cells. However, a detailed study on the synthesis of nanoparticles, nanowires, nanoclusters of various metals, and its alloys using electrodeposition technique has not been reported so far. Therefore, we have attempted to present a comprehensive overview encompassing the synthesis of nanoparticles, nanowires, and nanoclusters of various metals and their oxides, namely, Au, Pt, Ni, Fe, Ag etc. using electrodeposition techniques. The potential applications of these nanoscale materials are also described in this article. Various surface analytical techniques like SEM, TEM, XPS, FTIR, AFM, and electroanalytical methods like cyclic voltammetry, chronoamperometry, and chronopotentiometry have been employed for the characterization of the synthesized nanoparticles.

2 Synthesis and applications of nanoparticles, nanorods, nanoclusters of metals, and their alloys by electrodeposition technique

2.1 Gold

2.1.1 Gold nanoparticles and nanocomposites

El-Deab and co-workers [22, 23] used potential step electrolysis method to deposit Au nanoparticles (AU NPs) on a glassy carbon electrode (GCE) from an electrolytic bath that comprised $NaAuCl_4$ and H_2SO_4. Scanning electron microscopy (SEM) and X-ray diffraction (XRD) studies revealed that the electrodeposited Au nanoparticle having relatively short potential step width exhibited Au (111) plane as the predominant crystal orientation, and its particle size was greater than 100 nm. Ma et al. [24] employed cyclic voltammetric (CV) technique to electrodeposit Au on an ITO (indium tin oxide) glass electrode in the potentials ranging from -1.15 to -1.25 V for 20 cycles at a scan rate of 50 mV s^{-1}. A decrease in the deposition potential was noted in the cyclic voltammogram, thereby leading to an increase in the sensitivity from 76.4 to 183.5 A/mM. The shape of the GNP was found to be quasi-spherical, and its diameter was observed to be in the range of 20–60 nm from the SEM studies.

The role of GNPs in the modification of various electrodes and fabrication of different kinds of biosensors has been reported [25, 26]. Wang et al. [27] synthesized monodispersed GNPs on ITO-film-coated glass employing different electrodeposition techniques. CV studies revealed that a characteristic oxidation peak and a reduction peak were obtained at 1.28 and 0.81 V, respectively, indicating the successful deposition of GNPs on the ITO surface. Quasi-spherical shape of GNPs with particle size of 20–35 nm was established from the SEM studies. Also, the immobilization of superoxide dismutase (SOD) on GNP-modified ITO electrode resulted in an increase in catalytic activity. Huang et al. [28] demonstrated for the first time an easier and more convenient electrochemical method to prepare large number of well-dispersed GNPs with novel dumbbell structures in the aqueous phase with the help of surfactants; cetyl trimethyl ammonium bromide, and tetradecyltrimethylammonium bromide (TTABr) respectively. The authors found that the shape of GNPs can be modified to form dumbbell structures by addition of acetone solvent during the electrolysis. The shape of the nanoparticle changed from rod-shaped to dumbelled ones with increase in the injection rate of acetone solvent from 40 to 60 μL min^{-1}, as obtained from the TEM studies. The gold nanodumbells were found to be single crystalline with a face centered cubic (fcc) structure and exhibited an aspect ratio of around 3.

Apart from the metal nanoparticles, the preparation of composites of metal particles and conducting polymers with core–shell structure has also been of considerable importance to the scientists because of their interesting properties and potential applications in technological fields. The synthesis of gold/polypyrrole (Au/PPy) core–shell nanocomposites [29] by electrochemical methods has been reported. Ting [30] obtained Au/polyaniline nanocomposites with core–shell structure on the IT0 surface using electrochemical techniques. The results from the AFM (Atomic Force Microscopy) studies established that the GNPs with core–shell structure sizes of which varied from 250 to 300 nm fill coverage of 30-nm polyaniline shell that was present on the gold surface. Rapecki et al. [31] reported the synthesis of PPy–Au nanoparticle composites on the graphite surface from a solution comprising gold salt and monomer by pulse electrodeposition method. CV technique was used to determine the potential ranges of gold deposition and PPy formation and also for optimizing the conditions of the composite electrosynthesis. The peaks related to the reduction of $Au(CN)_2$ and the oxidation of pyrrole (Py) were observed at -1.5 and $+0.7$ V respectively. The composition and uniformity of the composites at the graphite surface was controlled by applying the

appropriate concentration of the reagent and pulsed deposition. This method provided an opportunity to deposit PPy–Au composites of any content including pure gold and pure polymer.

Shen et al. [32] developed a convenient, one-step facile pulse sonoelectrochemical method for the synthesis of Au NPs without using a reductant or a stabilizer. The size and shape of the Au NPs were controlled by adjusting current density, reaction time, and the pH value of the precursor solution. The average diameter of the GNPs varied from 20 to 30 nm, and the shape GNPs varied with changes in pH and reaction time. The Au NPs obtained were used as building blocks for fabrication of horseradish peroxidase (HRP) biosensor, which exhibited excellent biocatalytical activity with high sensitivity and rapid response. Since no surfactants/capping agent were used in the synthesis, the resulting Au NPs were suitable for potential applications in the field of biology and catalysis.

Chen et al. [33] reported a novel electrochemical route for the preparation of Au NPs incorporated in amorphous hydrogenated carbon films (a-C:H) films on single crystal silicon substrates. The sizes of the Au NPs were spherical, uniform, and well dispersed in the amorphous carbon as revealed by the TEM images. Results from X-ray photoelectron spectroscopy (XPS) and selected area electron diffraction (SAED) established the zero-valence crystalline phases of Au NPs with preferred orientation in the composite film. The authors also found that incorporation of Au nanoparticle in the carbon matrix drastically increased the electric conductivity indicating a rapid transition from an insulator to a semiconductor. This method served as an excellent model for different kinds of nanoparticles which can be spontaneously incorporated in an a-C:H film in the same way, so as to acquire excellent catalytic activity, special electronic. and optical properties.

Yu et al. [34] employed potentiostatic electrodeposition technique to synthesize pure (111) Au NPs of diameter 10 nm on bulk Au substrates in the presence of biopolymer chitosan (CS). CV studies revealed that $AuCl_4^-$ was readily adsorbed on CS as a precursor for the subsequent preparation of red Au NPs in solutions. The absorbance maxima appeared approximately, respectively, at 311 and 313 nm for prepared $AuCl_4^-$ in solutions with and without CS, which were markedly different from those of zero-valent Au NPs located at ca. 520 nm. The prepared Au NPs in solutions were capable for anti-oxidation and found to be stable in an ambient atmosphere for at least 3 months. The capabilities for anti-oxidation were evaluated by comparing the Au NPs containing sample solution with a fixed concentration of vitamin C, which could protect Prussian blue (PB) from oxidation. The experimental results demonstrated that the capability for anti-oxidation for 1 ppm Au NPs was equivalent to that of 0.12 ppm vitamin C.

2.1.2 *Gold nanorods*

The first electrochemical route to gold nanorod formation was developed by Chang et al. [35]. Electrodeposition studies were carried out at a current density of 3 mA cm^{-2} from an electrolytic bath composed of hexadecyltrimethylammoniumbromide (C16TAB) and tetradodecylammonium bromide (TC12AB). C16TAB stabilized the nanoparticles and prevented them from further aggregation. The length of the nanorods was also dependent on the concentration of gold ions and their release rate. Martin and co-workers [36–38] employed template method to synthesize gold nanorods. The method was based on the electrochemical deposition of gold within the pores of nanoporous polycarbonate or aluminum template membranes. Wang et al. [39] used nanoporous anodic alumina oxides (AAO) as templates for the electrodeposition of gold nanowires from an electrolytic bath composed of $HAuCl_4 \cdot 3H_2O$, Na_2SO_3, and K_2HPO_4. The gold nanowires formed were ductile, and the average diameter of the nanowires was found to be 180 nm m the SEM studies. The chemical state of gold in the nanowires was confirmed from the XPS and EDX spectra.

TEM results demonstrated a change in morphology from the tubular rod structure to solid nanorods structure with the increase in electrodeposition time from 150 to 270 s. Several authors have reported [40, 41] the growth of gold nanorod arrays inside commercial polycarbonate (PC) membrane templates of pore size 100 nm employing electrodeposition techniques. Lin et al. [42] used stainless steel sheet of 9-mm diameter as the working electrode and Pt mesh as the counter electrode for the electrodeposition experiments performed by cyclic voltammetry. XRD and SEM studies revealed that the as-synthesized gold nanorods were polycrystalline with unidirectional direction along [111] plane and had an uniform diameter of 100–200 nm. Disordered gold nanorods and 1D arrayed gold nanorod-modified (3D nanostructure) working electrodes were fabricated by this process. In addition, ordered 1D gold nanorod-modified electrodes exhibited more number of CV signals than that of disordered gold nanorod-modified electrodes. CV studies also demonstrated that 1D nanorods facilitated the electrocatalytic reactions because of enhanced diffusion occurring around these nano-structures. The advantages of using 1D gold nanorod-arrayed structures for the electrochemical sensing lay primarily on that the electrochemical processes proceeded with the highest efficiency because of the geometry of an exposed structure and large surface area.

Wang et al. [43–45] observed different crystallographic faces of gold nanorods with different aspect ratios prepared by the electrochemical method using high-resolution TEM (HRTEM). The results revealed that the short gold

nanorods prepared by the electrochemical method were single crystals with {110} and {100} as the dominant faces, while the long rods exhibited {111} and {110} planes as the dominant faces. Wang et al. [46, 47] have reported the growth of Au nanorod or nanowire arrays in templates using electrodeposition techniques. SEM studies on Au nanorod or nanowire arrays grown in templates established that both nanorod and nanotube arrays could be readily grown by varying the growth conditions, either to promote preferable growth along the surface of pore channels resulting in the formation of nanotube arrays, or to initiate deposition at the bottom of the pore channels attached to the electrode leading to the growth of nanorod arrays.

A simple electrochemical method for the synthesis of 1D crooked gold nanorods (CGNRs) and 2D gold network structures in the presence of isopropanol (IPA) solvent with ionic surfactant solution has been reported [48]. The CGNRs formed had many aspect ratio (γ) values, and surface plasmon absorption was red-shifted from 532 to 560 nm. HRTEM images demonstrated that the CGNRs were formed from many small gold nuclei aggregation between the large grains during the growth process, indicating that small gold nuclei linked the large gold grains. The gold network structure was obtained by interconnecting several CGNRs to form the interconnected network structures, which were observed with the almost-flat absorbance curves and broad peaks from 500 to 1,100 nm. This study demonstrated that the electrochemical method was suitable for low-cost, low-temperature, and rapid fabrication of GNPs.

2.1.3 Gold nanowires

Au, Ag, and Cu nanowires [49] with diameters ranging from 40 to 250 nm were synthesized by potentiostatic deposition method. Scanning electron micrographs revealed that the Au nanowires were 20–30 μm in length and 40–50 nm in diameter. This method of synthesis helped us to understand the aggregation process in various nanowire systems and properties of individual nanowires.

Lu et al. [50] synthesized gold nanowires by an electrodeposition technique using nanopore polycarbonate (PC) membrane, with the average diameter of the nanowires being 250 nm and length about 10 μm. The gold nanowires prepared were dispersed into CS solution and stably immobilized onto GCE surface. In this study, the authors investigated the electrochemical behavior of gold nanowire-modified electrode, and its application in the electrocatalytic reduction of hydrogen peroxide (H_2O_2) was studied. The modified electrode showed sensitive response toward hydrogen peroxide at −0.2 V with its sensitivity being better than that of the conventional gold electrode. The high sensitivity of the gold nanowire-modified electrode toward hydrogen peroxide, and the large surface area thus makes it ideal for the absorption of enzymes for the fabrication of biosensors. Glucose oxidase was made to be adsorbed onto the nanowire surface to result in the fabrication of glucose biosensor as an application example. The resulting biosensor exhibited good amperometric response to glucose. The biosensor fabrication method truly offered a promising platform for various biosensing applications.

The electrodeposition of gold nanowires from cyanide baths using polycarbonate templates with pore diameter of 80 nm has been reported [51]. Electrochemical methods were used to characterize the gold electrodeposition process and to investigate the nucleation and growth mechanism. Cyclic voltammograms demonstrated that the electrodeposition of gold nanowires took place under diffusion control. The authors observed that with decrease in gold concentration, the cathodic peaks shifted toward more negative potentials with lower current density confirming the diffusion controlled reduction of gold ions. Current transients revealed that nucleation mechanism was instantaneous with a typical three-dimensional (3D) nucleation growth process. The transition–time measurements showed that the gold electrodeposition occured as one-electron valence involved in the reaction mechanism. SEM micrographs revealed that nanowires had a laminar growth in different directions. However, owing to the spherical diffusion around the protrusions, a cauliflower-like growth was observed, which led to the formation of caps on the surface.

2.1.4 Gold nanoclusters

Li and Lin [52] synthesized gold nanoclusters (nano-Au) on ultrathin overoxidized polypyrrole film ($PPyo_x$)-modified glass carbon electrode (GCE) by electrodeposition technique which could be further used to develop a novel biosensor for selective and sensitive detection of epinephrine (EP) and uric acid (UA) in the presence of ascorbic acid (AA). CV studies revealed that nano-Au/$PPyo_x$/GCE exhibited a strong electrocatalytic activity toward the oxidation of EP, UA, and AA. Also, the modified electrode resolved the overlapping anodic AA, EP, and UA peaks into three well-defined peaks at about 10, 190, and 370 mV, respectively. Scanning electron (SE) micrographs established that the Au nanoclusters of diameter 80 nm were distributed homogenously on the $PPyo_x$ film. XPS analysis further demonstrated the formation of two peaks at 84.1 and 87.8 eV, corresponding to the Au $4f_{7/2}$ and Au $4f_{5/2}$ components, respectively.

Liu et al. [53] also employed electrodeposition technique to synthesize gold nanoclusters (Au Ncs) on phosphorous-incorporated tetrahedral amorphous carbon electrode (ta-c:p).

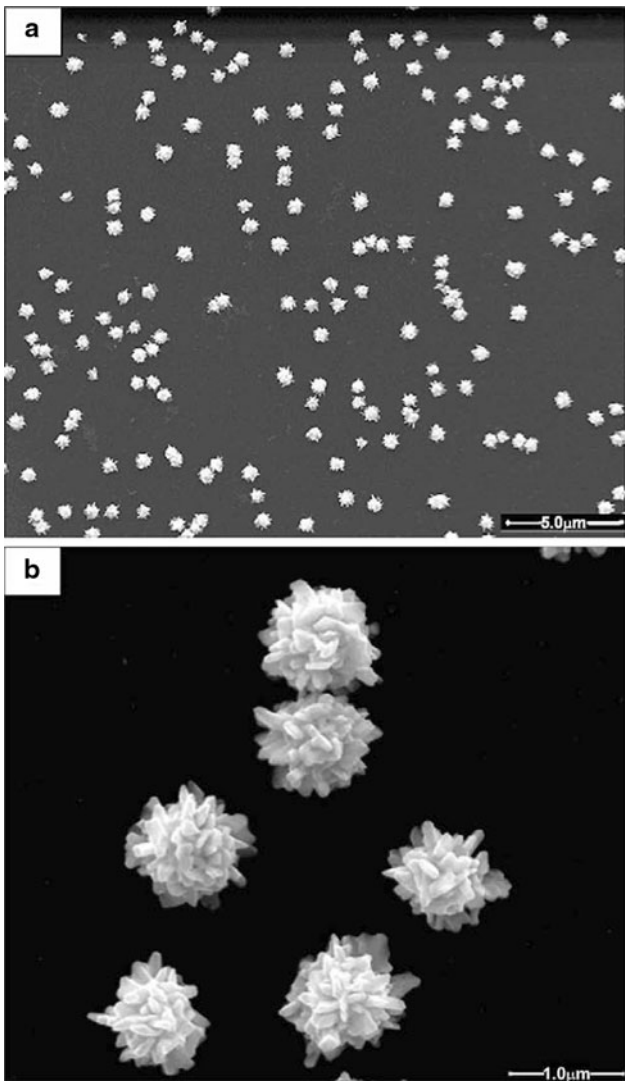

Fig. 1 Scanning electron micrographs of Au nanoclusters electrodeposited on GCE [54]

The reduction and oxidation peaks of Au being present at 0.16 and 1.14 V, respectively, was established from CV studies. SEM studies established the spherical shape of gold clusters for an electrodeposition time of 20 s, and the sizes of the Au Ncs varied from 13.5 to 75.7 nm. The electrodeposition of Au Nc on ta-c:p film enhanced the electrochemical activity toward ferricyanide oxidation, and this method also was found to have potential applications in electroanalysis systems. CV technique was used by Yang et al. [54] for the electrodeposition of Au Ncs on a GCE in the potential range of −0.8 to 0.6 V at a scan rate of 50 mV s^{-1}. Au Ncs formed had diameters of around 600 nm (Fig. 1a) with uniform distribution around the GCE surface. Flowerylike Au NCs composed of Au nanorods with an average diameter of 20 nm and a length of 80 nm were observed in the magnified images (Fig. 1b). The

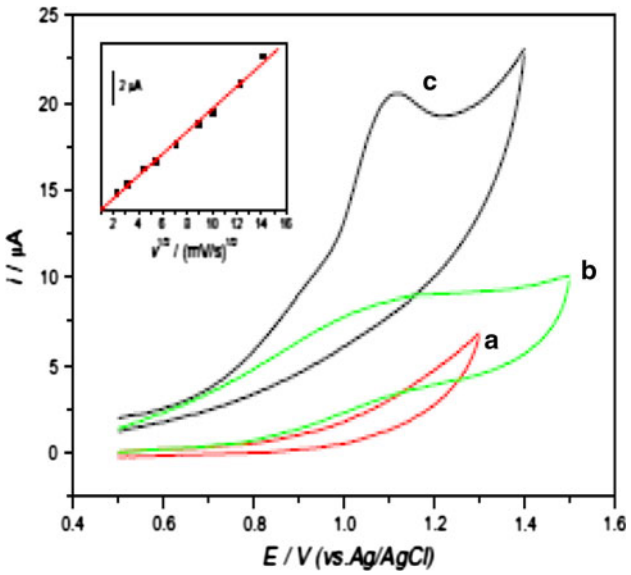

Fig. 2 Cyclic voltammograms of the bare GCE (*b*) and nano-Au/GCE (*a*, *c*) in the absence (*a*) presence of 4 ppm H_2S (*b*, *c*) in the supporting electrolyte at 30 mV s^{-1}. The *inset* shows the relationship between oxidation peak current and square root of the scan rate [54]

electrocatalytic oxidation of H_2S on the nano Au/GCE was investigated by CV studies. A broad anodic peak on the bare GCE (Fig. 2, curve b) and a sharp anodic peak at 1.1 V (Fig. 2, curve c) were observed with a significant increase in oxidation current thereby leading to a remarkable increase in the electron transfer of H_2S on the modified electrode surface.

2.2 Platinum

2.2.1 Pt nanoparticles

Electrodeposited Platinum (Pt) or platinum–ruthenium (Pt–Ru) nanoparticles on carbon nanotubes (CNTs) have been used as electrocatalyst materials for cathodes and anodes in low temperature fuel cells [55–57]. Tsai et al. [58] used ethylene glycol (EG) as a reducing agent for the electrodeposition of Pt and Pt–Ru nanoparticles on dense CNTs grown on carbon cloth (CC)—CNT/CC. EG enhanced the dechlorination of Pt and Ru precursor salts and led to the formation of nanoparticles. It also acted as a stabilizing surfactant and prevented the particles from agglomeration during the electrodeposition processes. The particle sizes of electrodeposited Pt nanoparticles on CNTs were ranging from ∼4.5 to ∼9.5 nm as revealed from TEM studies. The electrochemical tests performed on the working specimens revealed that the specimens with Pt–Ru catalysts exhibited better electroactivity than the specimens with only Pt. Also, the working specimen with Pt–Ru catalysts electrodeposited at −0.45 V SCE demonstrated

better electrochemical characteristics than the others in terms of mass activity and suppression of CO poisoning, and proved to be a better electrode for methanol oxidation.

Yu et al. [59] used a cost-effective electrodeposition technique to synthesize Pt nanoparticles on a GCE using water immiscible ionic liquid (IL) droplet supported on the electrode surface. The electrodeposition was performed on an IL droplet supported GCE at −1.5 V vs. Ag/AgCl for 500 s from an electrolytic bath composed of KPF_6 and H_2PtCl_6. From the CV studies, it was established that the oxidation of methanol occurred at a potential of 0.70 V in the positive scan and another oxidation peak occurred at 0.45 V in the reverse scan indicating the adsorption of various intermediate species onto Pt surface. The morphology of electrodeposited Pt nanoparticles was found to be uniform, and its particle size ranged from 300 to 400 nm in the SEM images. Lu and Zangari [60] used potentiostatic deposition method to synthesize Pt nanoparticles on highly oriented pyrolytic graphite (HOPG) from chloride-based electrolytes. Spontaneous Pt deposition with wide particle size distribution occured on HOPG at open-circuit potential but was suppressed using anodic bias of the substrate before and after deposition. AFM revealed spontaneous reduction and agglomeration of Pt when HOPG substrate was immersed in $PtCl_2$ solution. Furthermore, AFM studies indicated that Pt nanoparticles of larger size had a lower height/diameter ratio, and consequently smaller particles were approximately spherical while larger ones were more disk-like.

Saminathan et al. [61] electrodeposited Pt on in situ-grown MWCNTs/carbon paper at potentials of −0.3, −0.6, −1.2, −2.4, and −3.6 V vs. SCE, from a bath comprising chloroplatinic acid (60 g/L) and hydrochloric acid (10 g/L). SEM micrographs (Fig. 3) revealed that Pt nanoparticles decorated on the MWCNTs/carbon paper were highly uniform when the electrodeposition voltage was maintained at −0.6 V vs. SCE. The authors also noted that Pt electrodeposited at potentials of −0.3 and −0.6 V produced better coulombic efficiency and lower gas evolution than those electrodeposited, respectively, at potentials of −2.4 and −3.6 V,. The nanoparticles exhibited efficient fuel cell performance under various operating conditions. The fuel cell performance with a Pt loading of 0.13 mg Pt cm^{-2} (electrodeposited at 0.6 V) using Naflon-212 membrane as electrolyte showed a peak power density of ∼640 mW cm^{-2} at 80 °C and 101 kPa.

Hassan [62] investigated the effect of deposited Pt and Pt*x*–Sn*y* nanoparticles on Ti and Pt substrates by employing both potentiostatic and galvanostatic techniques. Results from cyclic voltammetry and chronoamperometric experiments revealed that small amount of Sn deposited with Pt enhanced the catalytic activity and stability of the prepared electrode. The authors also observed that modified Pt/Ti electrodes prepared by the two methods had comparable performance and enhanced catalytic activity toward methanol electro-oxidation compared to Pt/Pt and smooth Pt electrodes.

The electrodeposition of metals on polymer-modified surface has been an emerging area of research since last few years and the topic has been of considerable importance [63, 64]. Qian et al. [65] have reported the synthesis of Pt nanoclusters on the surface modified by poly(amidomine) dendrimer (PAMAM) using electrodeposition as a tool. In this study, G4-NH2 (amine-terminated fourth-generation polyamidoamine) was first assembled onto polysodium-*p*-styrensulfonate (PSS)/poly-diallyl methyl ammonium chloride/indium tin oxide (PDDA/ITO) surface and then Pt nanostructures were potentiostatically deposited on the G4-NH2 surface at a potential of −0.2 V. Field-emitted scanning microscopy (FE-SEM) images established that the nanoclusters formed consisted of small Pt nanoparticles, and the size of these Pt nanoclusters could be changed by controlling the electrodeposition time. The SE micrographs (Fig. 4a, b) revealed that the Pt nanostructures formed on PSSA/PDDA/ITO surface consisted of larger Pt nanoparticles with corrugated surface, while the Pt nanoparticles formed on the bare ITO surface were smooth. This method provided an ideal path for the synthesis of novel nanostructures by electrodeposition technique.

2.3 Nickel

2.3.1 Nickel nanoparticles

Zhu et al. [66] employed electrodeposition technique to synthesize Ni nanoparticle chains embedded in TiO_2 nanotubes. Potentiostatic mode of deposition was used for the synthesis at potentials ranging from −1.3 to −1.7 V from an electrolytic bath composed of titanium fluoride and nickel chloride. Secondary electron image (SEI) in Fig. 5a revealed that the TiO_2 nanotubes were highly ordered with an average outer diameter of about 250 nm. On the other hand, the BSE (Fig. 5b) image with enhanced atomic contrast demonstrated that the nickel nanoparticle particle chains were embedded in the nanotubes, and the length of the Ni chains in TiO_2 nanotubes was dependent on the deposition time. The formation of Ni nanoparticle chains in TiO_2 nanotubes was attributed to the generation of H_2 bubbles and their periodical evolution outside the TiO_2 nanotubes. This method opened a pathway for preparation of various nanoparticle chains embedded in nanotubes with tunable magnetic, electrical, and optical properties.

Heinig et al. [67] grew uniform-sized and dispersed nickel core–shell nanoparticles on PPy film using potentiostatic deposition from a nickel sulfate bath containing boric acid. The amount and type of the deposited Ni

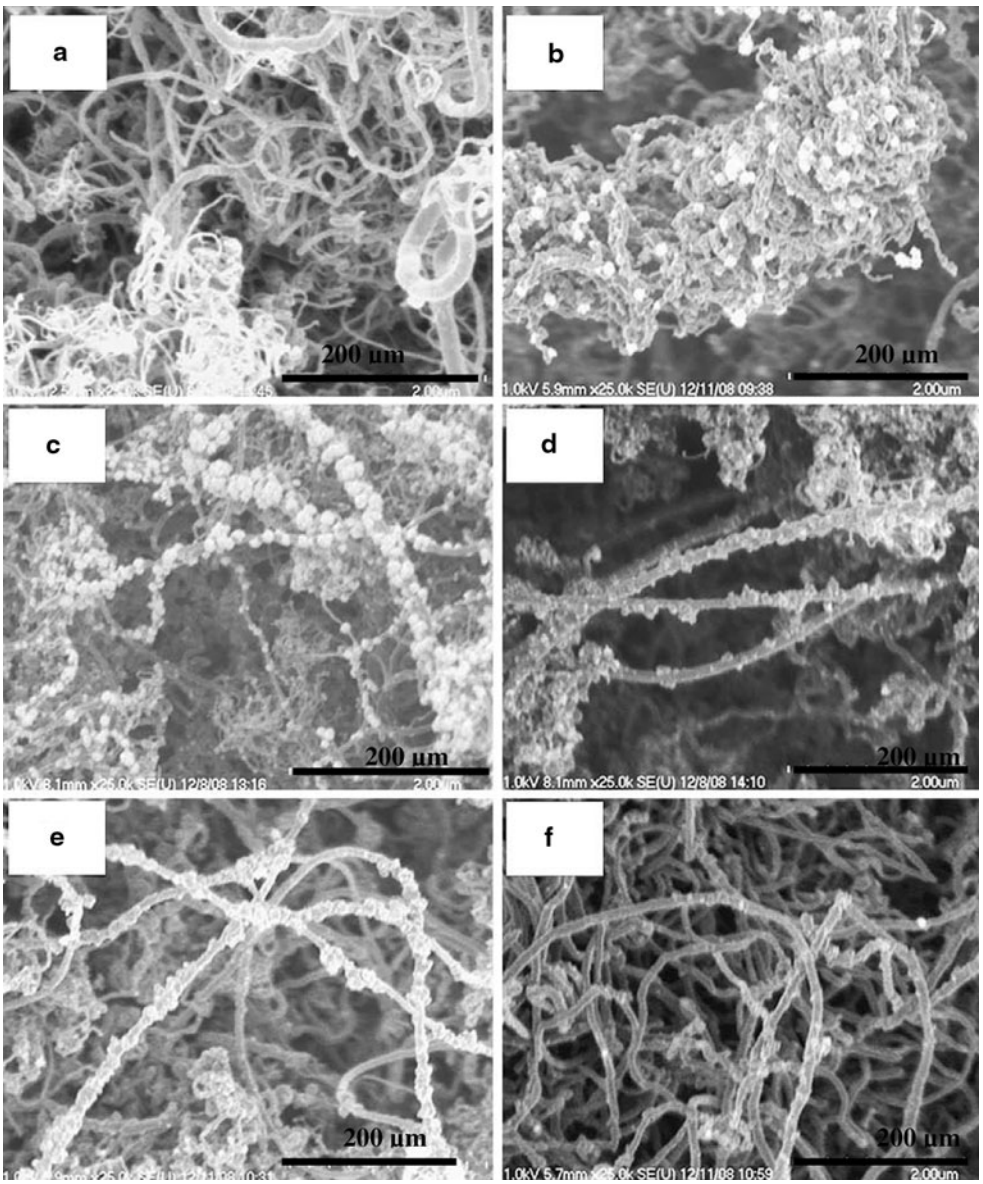

Fig. 3 Scanning electron micrographs of **a** pristine and **b–f** Pt deposited MWCNTs/carbon paper samples at various voltage values (L0.3, L0.6, L1.2, L2.4, and L3.6 V vs. SCE) [61]

nanoparticles were dependent on the preparation of the conducting polymer (PPy) substrate. The authors found that a 90–110-nm-thick PPy film grown on baked gold-coated silicon electrodes at or above 6 mA/cm^2 facilitated the deposition of Ni nanoparticles. The nanoparticles obtained had potential applications in nanocatalysis and quantum electronics. XPS analysis established that these nanoparticles were predominantly NiO.

2.3.2 Ni nanowires

Pirota et al. [68] obtained arrays of Ni nanowires of diameter 30 nm and separated by about 100 nm on to the pores of alumina membranes employing electrodeposition techniques. The nanoporous alumina membranes with hexagonal ordering were prepared by a two-step anodization process [69]. The fabrication and magnetic characterization of novel magnetic multilayer microwires have been investigated in this study. The multi-layered magnetic microwires were prepared in the following sequence: first a nanometric Au coat was sputtered onto Pyrex-coated FeSiB amorphous microwires, which was followed by electrodeposition of a 500-nm-thick Ni external cover. The noticeable influence of the Ni layer on the temperature dependence of hysteresis loops was also established from the studies. Both electrodeposited magnetic materials opened a bright opportunity for its use as sensing elements in various sensor devices.

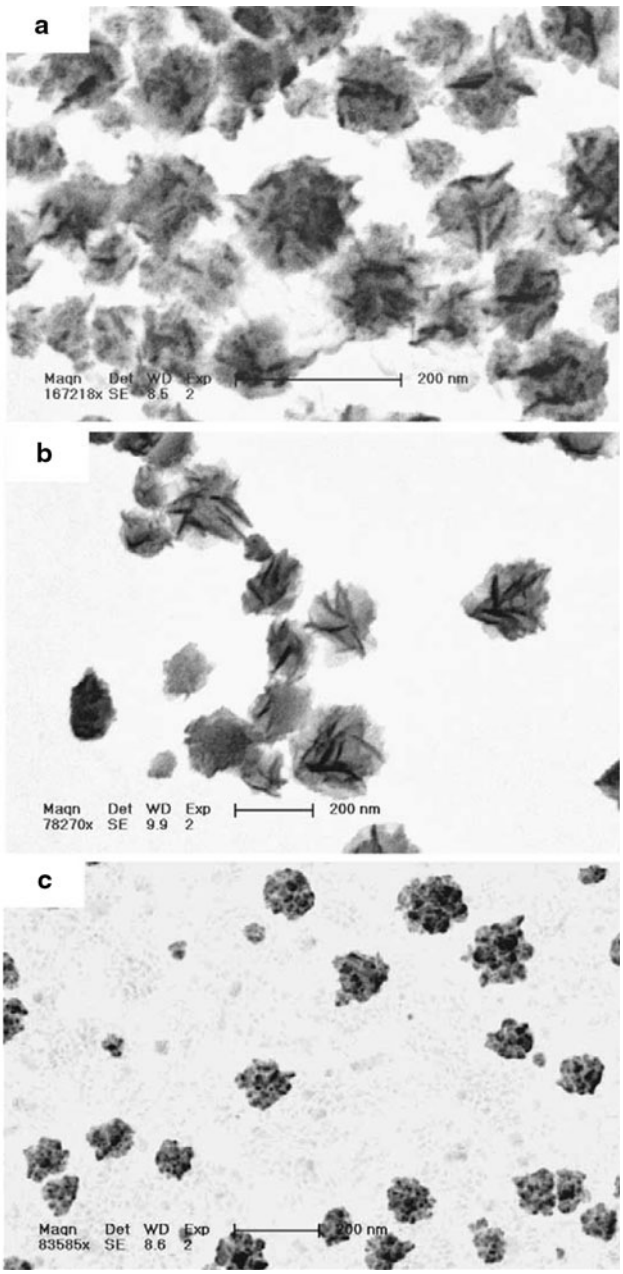

Fig. 4 FE-SEM images of Pt nanostructures prepared onto ITO surface electrodeposition potential of 0.2 V, time: 180 s; **a** bare ITO, **b** PSS/PDDA/ITO and **c** G4-H_2/PSS/PDDA/ITO [65]

Schönenberger et al. [70] grew Ni, Co, Cu, and Au nanowires using polycarbonate membranes with nominal pore diameters between 10 and 200 nm by an electrolysis method. Potentiostatic study of the growth process and SEM analysis of nanowires revealed that the pores in general were not cylindrical with a constant cross section but were rather cigar like. A direct electrochemical synthesis of oriented nanowires of polyaniline (PANI), a conducting polymer with its backbone conjugated by phenyl and amine groups, from solutions without using

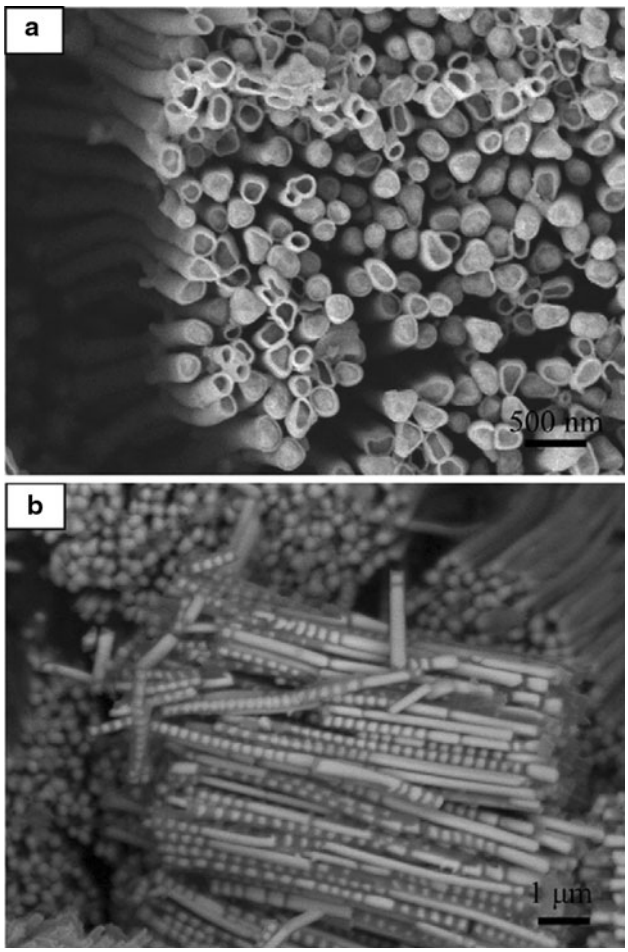

Fig. 5 Ni nanoparticle chains embedded in TiO_2 nanotubes electrodeposited from an electrolytic bath containing 0.04 M TiF_4 and 0.08 M $NiCl_2{\cdot}6H_2O$ at −1.50 V (vs. Ag/AgCl) for 10 min. **a** Top view SEI image of the nanotube arrays. **b** Side view BSE image of the Ni nanoparticle chains embedded in nanotubes [66]

templates have been reported [71]. The experimental design was based on the theory that the rate of electropolymerization (or nanowire growth) was related to the current density. The nucleation and the polymerization rate could, therefore, be controlled by adjusting the current density. The synthesis involved electropolymerization of aniline ($C_6H_5NH_2$) and in situ electrodeposition resulting in nanowire growth.

2.4 Prussian blue nanoparticles

The electrodeposition of PB nanoparticles on the CS nanofibers by potentiostatic technique has been reported [72] from an acidic solution containing single ferricyanide. The large surface-to-volume ratio of CS nanofibers facilitated larger contact of the PB nanoparticles with the medium and also provided more effective catalytic effect. In this study, CS nanofibers were successfully used to

modify ITO electrode by electrospinning technique. CV technique was used to investigate the CS nanofibers/PB nanoparticles system over potentials ranging from −0.2 to 1.2 V vs. Ag/AgCl at the pH value of 7.4. From the CV studies, two typical pairs of redox waves showing the oxidation of PB to Prussian green (PG) as well as the reduction to Prussian white (PW) were observed for the electrode modified with CS nanofibers/PB nanoparticles, indicating the presence of PB in the sample. Furthermore, it was established that the peak currents of the PB/ITO electrode (Fig. 6a) were smaller than that of the PB/ITO electrode modified with CS nanofibers (Fig. 6b) indicating high surface-to-volume ratio and large surface energy of the CS nanofibers. The PB nanoparticles also exhibited excellent electrochemical activity and electrocatalytic activity toward H_2O_2. This method provided a simple and promising way for local fabrication of compound on the nanofibers.

2.5 Iron

2.5.1 Iron and iron oxide nanoparticles

Iron cuboid nanoparticles supported on glassy carbon (denoted nm-Fe/GC) [73] were prepared by electrochemical deposition under CV conditions. Cyclic voltammograms demonstrated the formation of two oxidation current peaks at −1.03 and −0.69 V and two cathodic reduction peaks at −1.09 (D) and −1.21 V, respectively. The anodic process corresponded to the electrooxidation of Fe to Fe(II) and Fe(III) species [74] which might be FeOOH and some hematite and maghemite. CV studies also established that the Fe cuboid nanoparticles exhibited higher catalytic activity per unit surface area than that of bulk Fe toward electroreduction of nitrite. This enhanced catalytic activity might have originated from the open structure of the bcc {100] facets of the Fe nanocubes, or could be attributed to the size effects of Fe cuboid nanoparticles. The SE micrographs and SAED patterns in Fig. 7 reveal that the Fe cuboid nanoparticles were dispersed on the GC (glassy carbon) substrate with an average particle size of 171 nm.

A simple method for the electrochemical deposition of crystalline maghemite (Fe_2O_3) nanoparticles by cathodic reaction at room temperature in environmentally benign aqueous electrolytes was demonstrated by Park et al. [75]. Since iron oxide nanoparticles were electrodeposited in naturally aerated solution, two competitive electrochemical reactions occured at the cathode. One is the reduction of dissolved oxygen which combined with ferric ions to form Fe_2O_3. Another possible reaction was via hydrogen gas evolution, which caused an increase in local pH on the cathode surface and promoted the formation of ferric hydroxides which were later converted to form Fe_2O_3. The shape and size of nanoparticles were strongly dependent on the electrolyte composition and applied current density. Dendritic maghemite nanostructures with approximately 800–1,200-nm-thick trunks and 50–210-nm-thick branches were synthesized at a current density 150 mA cm^{-2}; while spherical shaped nanoparticles were observed in TEM micrographs with increase in concentration and current density. The greater adsorption kinetics of maghemite nanoparticles toward As (V) as compared to zero-valent iron nanoparticles was ascribed to its higher specific surface area. The applications of maghemite ranged from its use as a magnetic recording material to treatment of tumors in the form of ferrofluids hyperthermia [76, 77].

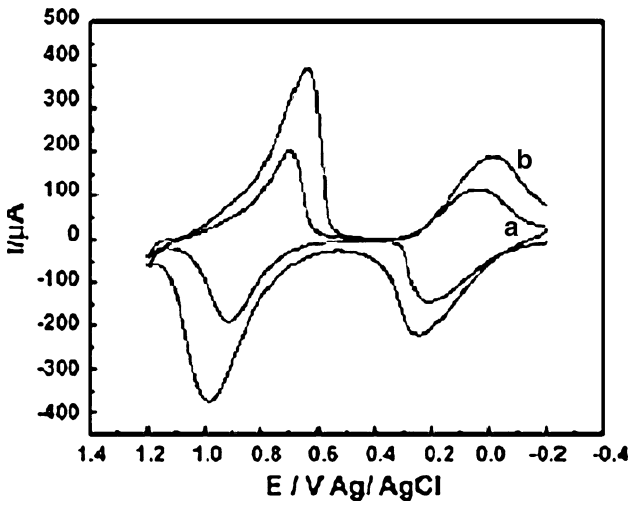

Fig. 6 Cyclic voltammograms of the ITO electrode modified with electrodeposited PB (*a*) and CS nanofibers/PB nanoparticles (*b*) in pH 7.4 PBS at a scan rate: 50 mV s^{-1} [72]

2.6 Silver

2.6.1 Synthesis of Ag nanoclusters

Isse et al. [78] employed a potentiostatic single-pulse technique to synthesize silver nanoclusters on glassy carbon (GC) from an electrolytic bath composed of CH_3CN, $LiCO_4$, and 1–2 mM $AgClO_4$. The potentiostatic deposition of silver particles on GCE was accomplished by pulsing the potential from 0.5 to −0.4 V vs. Ag/Ag^+. Under these conditions, the process was diffusion controlled and instantaneous nucleation of Ag occured on the GC surface. SEM images of Ag particles deposited on GC at the same potential and different deposition times revealed that the particles were spherical in shape and uniformly distributed over the GC surface. The Ag clusters exhibited remarkable electrocatalytic activity for the reduction of benzyl chloride. Ag/GC electrodes of suitable active surface can be employed in macroscale electrolyses

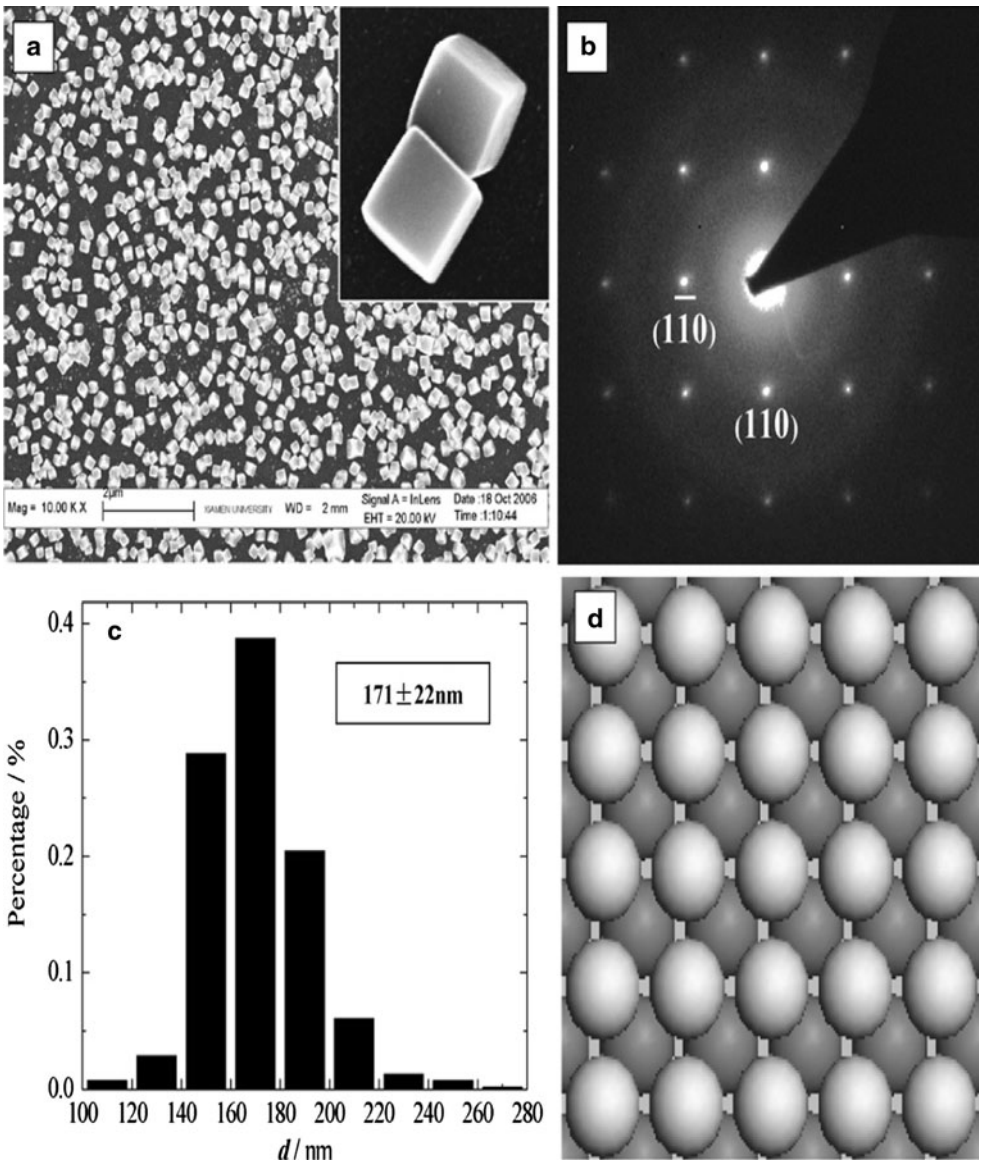

Fig. 7 **a** A typical SEM image of nm-Fe/GC electrode, the *inset* to this figure illustrates two Fe nanocubes with high magnification; **b** SAED pattern of a single Fe cube; **c** Histogram of size distributions of Fe nanocubes on GC substrate; **d** Model of bcc {100} plane that shows the open surface structure of Fe nanocubes [73]

for important catalytic electrosyntheses. Hussain and Pal [79] used galvanostatic technique to synthesize nanocrystalline silver on a Si substrate from an electrolytic bath composed of acetonitrile and silver acetate. SEM images revealed a change in the morphologies of silver nanoparticles with variations in size and volume fraction (Fig. 8). The images showed that the silver nanoparticles resided preferentially on the surface of the nanotubes, and the CNTs were branched in lamellar form with more densely populated silver nanoparticles on the surface of the CNTs (Fig. 8c, d). This surface deposited silver nanoparticle on CNTs served as an efficient and potent surface in catalysis applications. FTIR spectra for CNT films demonstrated that the peak for the vibrational modes of CNTs shifted toward higher frequencies while the shift was lower for films with lower concentration of silver nanoparticles.

2.6.2 *Synthesis of silver nanowires*

Both galvanostatic and potentiostatic methods were used to synthesize Ag nanowires [80] from a non-aqueous solution of $NaNO_3$ in ethanol. The electrolysis was performed galvanostatically using three silver anodes and two silver wires as cathodes situated half-distance between anodes at a current density of 0.5 mA cm^{-2}. On the other hand, the potentiostatic method used silver rod as a working electrode, a Pt plate as a counter-electrode and Ag/AgCl as a reference electrode. The authors proposed a mechanism which indicated that both anodic dissolution of silver and its reduction to metallic state proceeded during polarization in ethanol. Electron diffraction studies revealed the fcc crystal structure of metallic silver. This method reported was simple, required no expensive instruments and neither

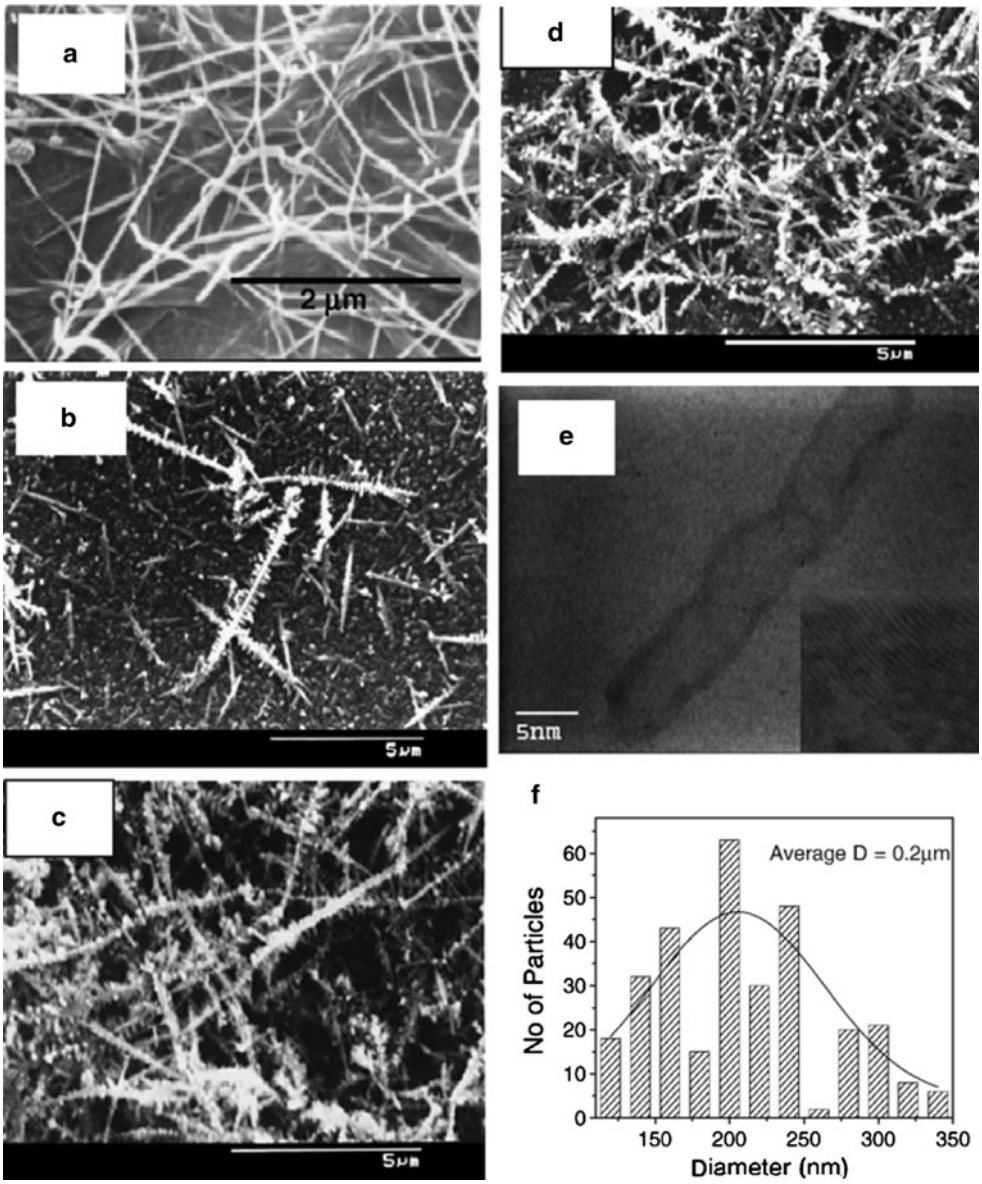

Fig. 8 SEM pictures of CNT film deposited: **a** without any silver, **b** *N*/1,000 Ag, appear in **c** *N*/6,000 Ag, **d** *N*/8,000 Ag, **e** HRTEM picture and **f** histogram corresponding to **d** [79]

surfactants nor additional reducing agents were needed. El-Abedin and Endres [81] synthesized nanocrystalline silver films and nanowires from the IL 1-ethyl-3-methylimidazolium trifluoromethylsulfonate using electrodeposition technique. Track-etched polycarbonate membranes with pore diameters of 100 nm were used as templates for the synthesis of Ag nanowires. CV studies (Fig. 9) indicated the presence of oxidation and reduction peaks corresponding to the deposition and stripping of silver. The presence of large amount of agglomerated crystallites in the range of 0.5–1 µm in size was obtained from the SEM micrographs. The present method established that ILs could provide environmentally benign conditions for electroplating.

Dalchiele et al. [82] synthesized silver nanowire arrays with high aspect ratios in the hollow structures of nanoporous templates using potentiostatic electrodeposition technique. The authors used two types of material as templates: commercial porous anodic aluminum oxide (with a mean pore diameter of 180 nm) and track-etched polycarbonate membranes (with a mean pore diameter of 15, 30 and 80 nm) respectively. The results showed that nanowires embedded in the AAO template exhibited a preferred crystallographic orientation along the [220] direction, while those in the PC template exhibited a [111] orientation. In both the cases, the corresponding textures were enhanced as the overpotential was increased. TEM images demonstrated that the nanowires grown on 180 nm AAO and 30 nm PC templates were straight, continuous, and dense with uniform diameter of 180 and 60 nm, respectively, while nanowires electrodeposited on the 80 nm PC template had a cigar-like shape.

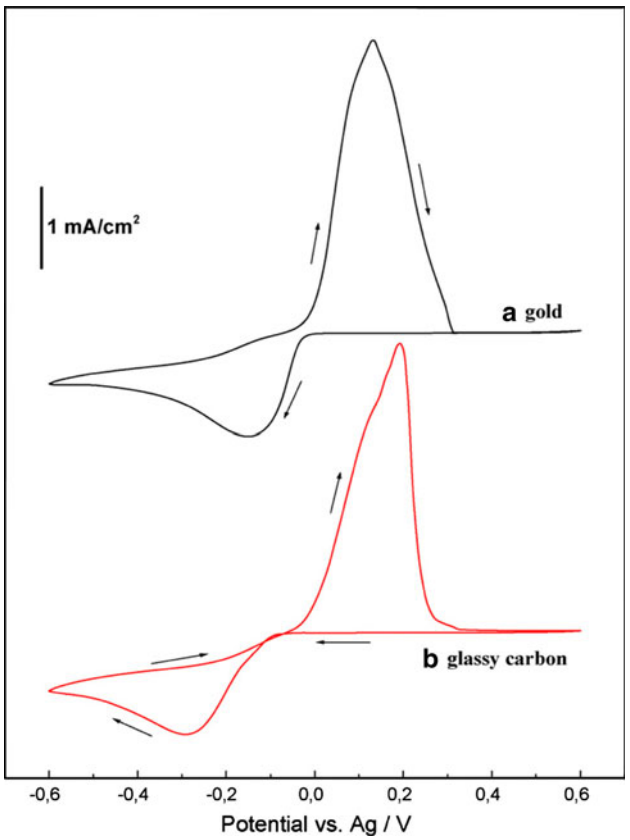

Fig. 9 Cyclic voltammograms of the ionic liquid [EMIm]TfO containing 0.2 mol/l Ag (TfO) recorded on (*a*) gold and (*b*) glassy carbon at a scan rate of 10 mV s^{-1} [81]

2.6.3 C_{60} nanoparticle

Hu et al. [83] have reported the synthesis of C_{60} nanoparticle-doped carbon film by electrodeposition technique. The electrodeposition set-up consisted of a silicon wafer as the working electrode and Pt plate as the counter electrode with methanol chosen as the electrolyte. TEM images revealed the presence of small dark spots and light features corresponding to C60 nanoparticles and carbon matrix, respectively. It was also noticed that C60 nanoparticles (5–7 nm in size) were well doped into the carbon film, and the doped films were continuous. The Raman spectrum for C60 nanoparticles exhibited three peaks at around 1,418, 1,459, and 1,585 cm^{-1} corresponding to Hg, Ag, and Hg vibration modes of C60 molecules, respectively. The incorporation of C60 decreased internal stress, and increased hardness and elasticity of the carbon films, indicating that C60 was a powerful dopant used for enhancing the mechanical properties of the carbon films. The above studies established that electrodeposition is a simple and efficient approach to incorporate C60 into carbon films, which is impossible for vapor deposition methods usually employed to fabricate carbon films.

2.7 Cobalt

2.7.1 Cobalt nanoclusters

Rivera et al. [84] investigated the morphology and magnetic properties of cobalt nanoclusters obtained from two different electrolytic sulfate baths. The cobalt nanoclusters were formed on HOPG by potentiostatic deposition from electrolytic baths composed of $CoSO_4 + Na_2SO_4$ and $CoSO_4 + 1\ M(NH_4)_2SO_4$. The clusters exhibited different diameters and heights which were dependent on starting electrolyte solution. The intrinsic properties of the ions employed in the formation process determined the kinetic behavior of the electrodeposition process, the size and magnetic distribution of the aggregates. The topographic images from AFM indicated the presence of aggregates of different size on the electrode surface, with the diameter and height ranging from 50–1,000 and 5–400 nm respectively.

2.7.2 Copper nanowires

Molares et al. [85] demonstrated direct current (DC) potentiostatic deposition of single-crystalline copper nanowires in etched ion track membranes using a simple-salt electrolyte. They achieved an aspect ratio of 500 by growing such needles with length of 30 μm and diameters as small as 60 nm. Homogeneous large-density arrays up to 10^9 wires/cm^2 were produced by this method. This method of synthesizing nanowires opened up the possibility of comparing nanometer-scale characteristics of poly and single-crystallinity with respect to electric current flow, acoustic wave propagation, and other transport phenomena.

2.8 Nanotube arrays and nanowires

2.8.1 RuO_2 nanotube arrays

Electrochemical deposition has also been explored for the synthesis of conductive polymer nanowire and nanorod arrays [86]. Similar to metals, semiconductors, and conductive polymers, some oxide nanorod arrays can be directly grown from solutions by electrochemical deposition. Hydrous RuO_2 nanotube arrays were synthesized by means of template-assisted anodic deposition from an aqueous solution of 10 mM $RuCl_3$ and 0.1 M CH_3COONa [87]. Crystalline RuO_2 nanotube arrays were readily obtained by annealing at elevated temperatures. The specific power and specific energy of $RuO_2{\cdot}xH_2O$ nanotubular arrayed electrodes were found to be 4,320 kW kg^{-1} and 7.5 W h kg^{-1}, respectively, thus achieving the perfect performance for next generation supercapacitors.

2.8.2 ZnO nanowire

ZnO nanowire arrays were fabricated by one-step electrochemical deposition technique based on ordered nanoporous alumina membranes [88]. ZnO nanowire array was uniformly assembled into the nanochannels of anodic alumina membranes, and consists of single crystal particles.

2.8.3 Polypyrrole nanowires

A new electrochemical method for the synthesis of conducting PPy nanowires has been reported by Jerome and Jerome [89]. The authors used electrografting reaction to prepare a new substrate which can act as a template for the electropolymerization of Py to give nanowires. SEM studies established that the PPy wire had a diameter of approximately 600 nm and a length of about 300 mm. The nanowire formation was actually controlled by the complex interaction of several parameters, including PPy conductivity, current density, PPy and Py diffusion rates through the swollen layer of grafted polymers.

3 Conclusions

An overview of the synthesis of nanoparticles, nanowires and nanoclusters of various metals, metal oxides, namely, Au, Ag, Pt, Ni, ZnO, etc. by electrodeposition technique is presented in this article. Both potentiostatic and galvanostatic deposition methods were used for the synthesis of nanoparticles. The electrochemical behavior of various nanoparticles/nanowires/nanocomposites deposited on different substrates was investigated by cyclic voltammetry, chronoamperometry, and pulsed sonoelectrochemical techniques. Surface analysis techniques like XPS, TEM, SEM, XRD, FTIR, and Raman spectroscopy were used for the characterization of the synthesized nanoparticles. The potential applications of nanoparticles such as the role of one-dimensional gold nanoarrayed structures in electrochemical sensing, the use of gold nanowires in fabrication of biosensors, the importance of nickel core–shell nanoparticles in nanocatalysis and the role of maghemite in the treatment of tumors, etc. are well documented. This article has demonstrated that electrodeposition is indeed an inexpensive and versatile technique for the synthesis of novel nanostructures of various metals and its oxides.

Acknowledgments The author thanks the Head of the Department and Dr. Suresh Reddy for their encouragement and support during the preparation of the article.

References

1. Wieckowski A, Savinova ER, Vayenas CG (2003) Catalysis and electrocatalysis at nanoparticle surfaces. Marcel Dekker Inc., New York
2. Ozin G, Arsenault A (2005) Nanochemistry: a chemistry approach to nanomaterials. Springer, New York
3. Daniel MC, Astruc D (2004) Chem Rev 104:293
4. Kolb D, Simeone FC (2005) Electrochim Acta 50:2989
5. Bayoumi FM, Ateya BG (2006) Electrochem Commun 8:38
6. Lee HY, Kim SW, Lee HY (2001) Electrochem Solid State Lett 4A:19
7. Hong MS, Lee SH, Kim SW (2002) Electrochem Solid State Lett 5A:227
8. Cote LJ, Teja AS, Wilkinson AP, Zhang ZJ (2003) Fluid Phase Equilib 210:307
9. Fu X, Yu H, Peng F, Wang H, Qian Y (2007) Appl Catal A 321:190
10. Spatz J, Mossmer S, Moller M (1996) Chem Eur J 2:1552
11. Glass R, Moller M, Spatz JP (2003) Nanotechnology 14:1153
12. Esparza R, Rosas G, Fuentes ML, Sánchez RJF, Pal U, Ascencio JA, Pérez R (2007) Mater Charact 58:694
13. Serrano JG, Pal U (2003) Int J Hydrog Energy 28:637
14. Yang S, Zhang T, Zhang L, Wang S, Yang Z, Ding B (2007) Colloids Surf A 296:37
15. Lu DL, Tanaka KI (1996) J Phys Chem 100:1833
16. Huang H, Yang X (2005) Colloids Surf A 255:11
17. Finot MO, Braybrook GD, McDermott MT (1999) J Electroanal Chem 466:234
18. Srinivasan V, Weidner JW (1997) J Electrochem Soc 144L:210
19. Guo S, Wang E (2007) Anal Chim Acta 598:181
20. Riley DR (2002) Curr Opin Colloid Interface Sci 7:186
21. Rao CRK, Trivedi DC (2005) Coord Chem Rev 249:613
22. El-Deab MS, Okajima T, Ohsaka T (2003) J Electrochem Soc 150:A851
23. El-Deab MS (2009) Electrochim Acta 54:3720
24. Ma Y, Di J, Yan X, Zhao M, Lu Z, Tu Y (2009) Biosens Bioelectron 24:1480
25. Yanez SP, Pingarron JM (2005) Anal Bioanal Chem 382:884
26. Welch CM, Compton RG (2006) Anal Bioanal Chem 384:601
27. Wang L, Mao W, Ni D, Di J, Wu Y, Tu Y (2008) Electrochem Commun 10:673
28. Huang CJ, Chiu PH, Wang YH, Yang CF (2006) J Colloid Interf Sci 303:430
29. Liu YC, Chuang TC (2003) J Phys Chem B 107:12383
30. Ting L (2007) Trans Nonferr Met Soc China 17:1343
31. Rapecki T, Donten M, Stojek Z (2010) Electrochem Commun 12:624
32. Shen Q, Min Q, Shi J, Jiang L, Hou W, Zhu J (2011) Ultrason Sonochem 18:231
33. Chen G, Zhang J, Yang S (2007) Electrochem Commun 9:1053
34. Yu CC, Liu YC, Yang KH, Li CC, Wang CC (2010) Mater Chem Phys (in press)
35. Chang SS, Shih CW, Chen CD, Lai WC, Wang CRC (1999) Langmuir 15:701
36. Foss CA Jr, Hornyak GL, Stockert JA, Martin CR (1992) J Phys Chem 96:7497
37. Martin CR (1994) Science 266:1961
38. Martin CR (1996) Chem Mater 8:1739
39. Wang HJ, Zou CW, Yang B, Lu HB, Tian CX, Yang HJ, Li M, Liu CS, Fu DJ, Liu JR (2009) Electrochem Commun 11:2019
40. Shingubara S, Okino O, Sayama Y, Sakaueand H, Takahagi T (1997) Jpn J Appl Phys 36:7791
41. Motoyama M, Fukunaka Y, Sakka T, Ogataand YH, Kikuchi SE (2005) J Electroanal Chem 584:84

42. Lin CC, Juo TJ, Chen YJ, Chiou CH, Wang HW, Liu YL (2008) Desalination 233:113
43. Wang ZL, Gao RP, Nikoobakht B, El Sayed MA (2000) J Phys Chem B 104:5417
44. Wang ZL, Mohamed MB, Link S, El Sayed MA (1999) Surf Sci 440:809
45. Wang ZL (2000) J Phys Chem B 104:1153
46. Wang JG, Tian ML, Mallouk TE, Chan MH (2004) J Phys Chem B 104:841
47. Wang HW, Russo B, Cao GZ (2006) Nanotechnology 17:2689
48. Huang CJ, Chiu PH, Wang YH, Yang CF, Wei FS (2007) J Colloid Interf Sci 306:56
49. Wu B, Boland JJ (2006) J Colloid Interf Sci 303:611
50. Lu Y, Yang M, Qu F, Shen G, Yu R (2007) Bioelectrochemistry 71:211
51. Soleimany L, Dolati A, Ghorbani M (2010) J Electroanal Chem 645:28
52. Li J, Lin XQ (2007) Anal Chim Acta 596:222
53. Liu A, Zhu J, Han J, Wu H, Jiang C (2008) Electrochem Commun 10:827
54. Yang B, Wang S, Tian S, Liu L (2009) Electrochem Commun 11:1230
55. Rajesh B, Thampi KR, Bonard JM, Xanthopoulos N, Mathicu HJ, Viswanathan B (2003) J Phys Chem B 107:2701
56. Liu Z, Gan LM, Hong L, Chen W, Lee JY (2005) J Power Sources 139:73
57. Mu Y, Liang H, Hu J, Jiang L, Wan L (2005) J Phys Chem B 109:22212
58. Tsai MC, Yeh TK, Tsai CH (2006) Electrochem Commun 8L:1445
59. Yu P, Yan J, Zhang J, Mao L (2007) Electrochem Commun 9:1139
60. Lu G, Zangari G (2006) Electrochim Acta 51:2531
61. Saminathan K, Kamavaram V, Veedu V, Kannan AM (2009) Int J Hydrog Energy 34:3838
62. Hassan HB (2009) J Fuel Chem Technol 37:23
63. Ye JH, Fedkiw PS (1996) Electrochim Acta 41:221
64. Baunach T, Ivanova V, Kolb DM, Boyen HG, Ziemann P, Buttner M, Oelhafen P (2004) Adv Mater 16:2024
65. Qian L, Liu Y, Song Y, Li Z, Yang X (2005) Electrochem Commun 7:1209
66. Zhu W et al (2009) Electrochim Acta. doi:10.1016/j.electacta.2009.08.059
67. Heinig NF, Kharbanda N, Pynenburg MR, Zhou XJ, Schultz GA, Leung KT (2008) Mater Lett 62:2285
68. Pirota K, Navas D, Vélez MH, Nielsch K, Vázquez M (2004) J Alloy Compd 369:18
69. Masuda H, Fukuda K (1995) Science 268:1466
70. Schönenberger C, van der Zande BMI, Fokkink LGJ, Henny M, Schmid C, Krüger M (1997) J Phys Chem B101:5497
71. Liang L, Liu J, Windisch CF, Exarhos GJ, Lin Y (2002) Angew Chem Int Ed Engl 41:3665
72. Shan Y, Yang G, Gong J, Zhang X, Zhu L, Qu L (2008) Electrochim Acta 53:7751
73. Chen Y, Chen SP, Chen QS, Zhou ZY, Sun SG (2008) Electrochim Acta 53:6938
74. Cuesta A, Gutirrez C (1996) J Phys Chem B 100:12600
75. Park H, Ayala P, Deshusses MA, Mulchandani A, Choi H, Myunga NV (2008) Chem Eng J 139:208
76. Hu J, Chen G, Lo IMC (2006) J Environ Eng 132:709
77. Lee SJ, Jeong JR, Shin SC, Kim JC, Kim JD (2004) J Magn Magn Mater 282:147
78. Isse AA, Gottardello S, Maccato C, Gennaro A (2006) Electrochem Commun 8:1707
79. Hussain S, Pal AK (2008) Mater Lett 62:1874
80. Starowicz M, Stypuła B, Banas J (2006) Electrochem Commun 8:227
81. El Abedin SZ, Endres F (2009) Electrochim Acta 54:5673
82. Dalchiele EA, Marottia RE, Cortes A, Riveros G, Gomez H, Martinez L, Romero R, Leinen D, Martin F, Ramos-Barrado JR (2007) Physica E 37:184
83. Hu H, Chen G, Zhang J (2008) Carbon 46:1095
84. Rivera M, Rios-Reyes CH, Mendoza-Huizar LH (2008) Appl Surf Sci 255:1754
85. Molares MET, Buschmann V, Dobrev D, Neumann R, Scholz R, Schuchert IU (2001) Adv Mater 13:62
86. Yi G, Schwarzacher W (1999) Appl Phys Lett 74:1746
87. Hu CC, Chang KH, Lin MC, Wu YT (2006) Nano Lett 6:2690
88. Zheng MJ, Zhang LD, Li GH, Shen WZ (2002) Chem Phys Lett 363:123
89. Jerome R, Jerome C (1998) Angew Chem Int Ed 37:215